Extended Data Figure 1

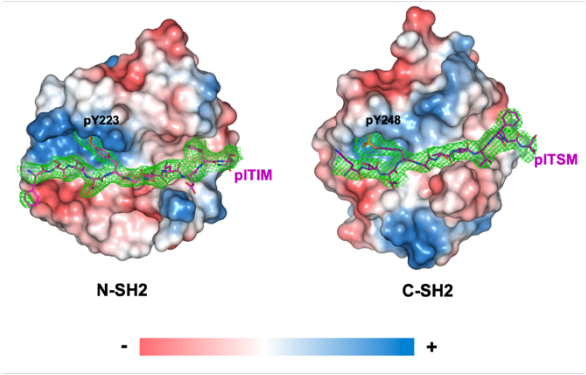

Extended Data Fig. 1 | Omit maps (green mesh) of pITIM and pITSM contoured at 1.5 σ. Electrostatic surface charge of N-SH2 (left) and C-SH2 (right) domains is also displayed.

Extended Data Figure 2

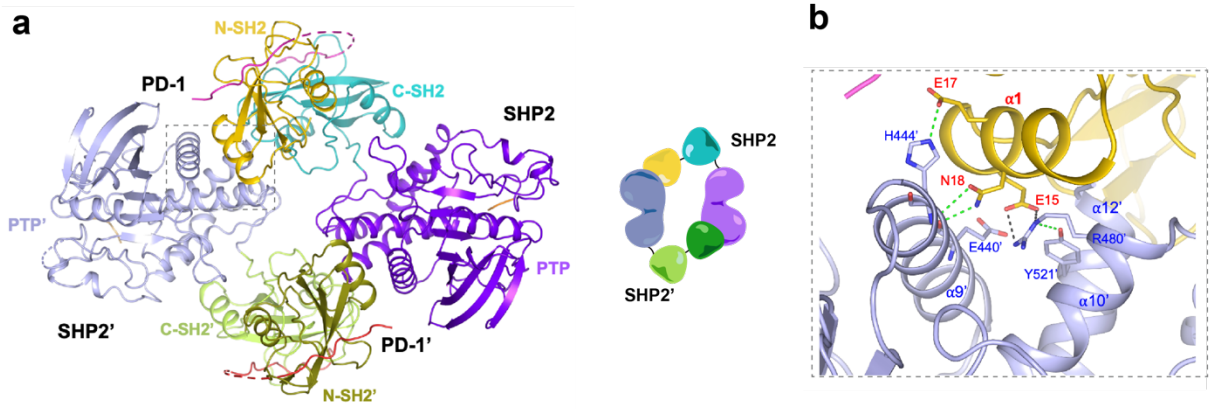

Extended Data Fig. 2 | Dimeric SHP2–PD1 motif complex structure. a, Dimeric SHP2-PD1 motif complex structure observed in crystal. **b**, Close-up view of the interface between SHP2 N-SH2 with the PTP domain from the other SHP2 molecule in the dimer. Green dashed lines indicate hydrogen bonds, grey dashed lines indicate salt bridges. SHP2 shown here is core SHP2 (residues 1–525) carrying the C459S mutation. pITIM motif (residues: 218–234, sequence: VFSVDpYGELDFQWREKT), and pITSM motif (residues: 242–256, sequence: VPEQTEpYATIVFPSG).

Extended Data Figure 3

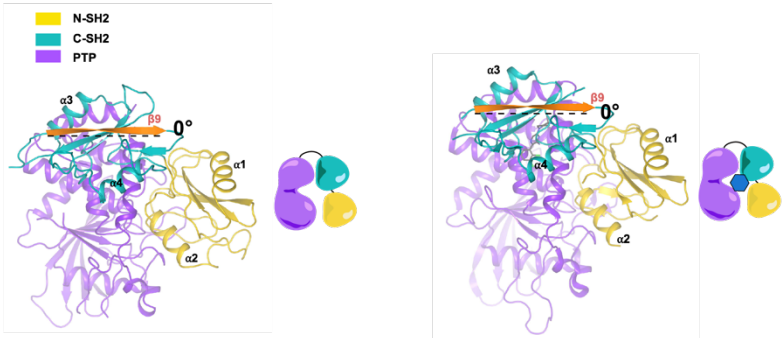

SHP2 SHP2+SH099

Extended Data Fig. 3 | Crystal structures of SHP2 alone (PDB: 2SHP) or in complex with the allosteric inhibitor SHP099 (PDB: 5EHR). β9 in the C-SH2 domain is colored orange to highlight the orientation of the C-SH2 domain, and the rotation degree is labelled. SHP2 shown here is core SHP2 (residues: 1–525).

Extended Data Figure 4

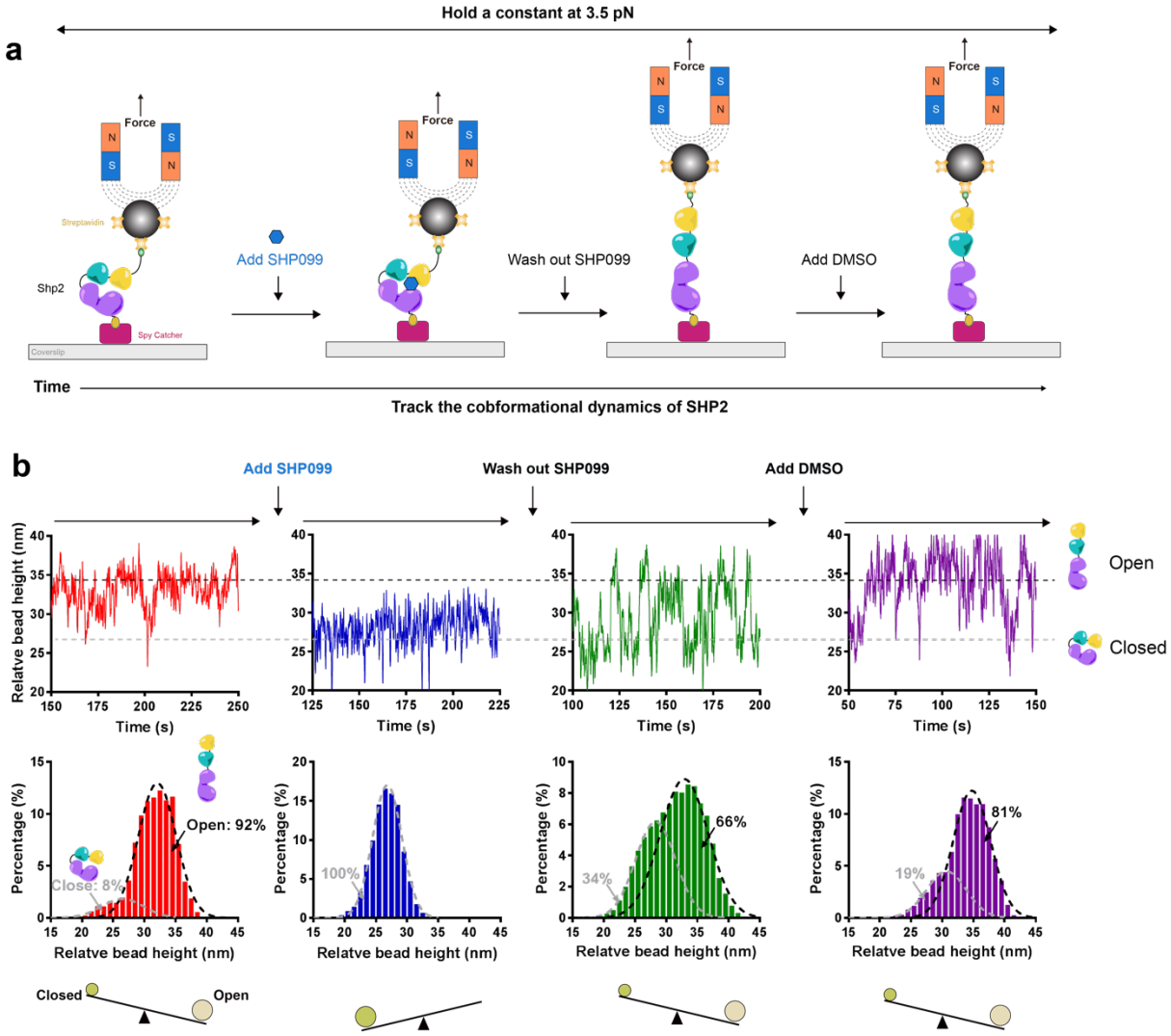

Extended Data Fig. 4 | The allosteric inhibition of SHP099 on SHP2 is reversible. a, The diagram of using the MT to track the dynamics of conformational changes of SHP2 with or without SHP099 under 3.5 pN constant force, SHP2 with DMSO serves as the control to eliminate the effect of DMSO on the SHP2 conformations. **b**, The dynamics of conformational changes of SHP2 with or without SHP099. Although the experiments were conducted continuously before and after each group, the time axis for each graph was reset, and a 100-second segment was selected for display. SHP2 shown here is core SHP2 (residues: 1–525).

Extended Data Figure 5

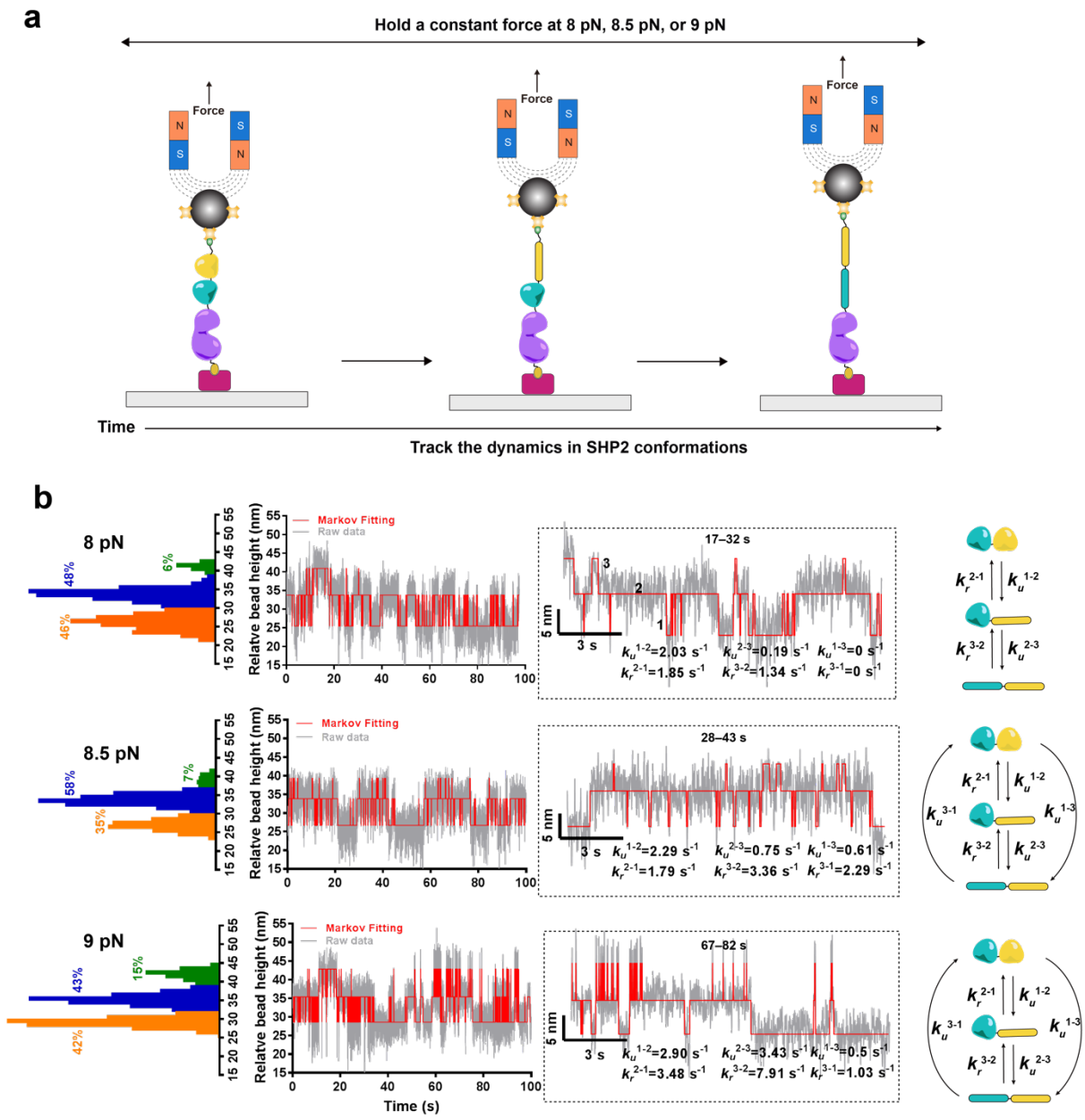

Extended Data Fig. 5 | The unfolding and refolding conformational switch of the N-SH2 and C-SH2 domains in SHP2 is captured and quantified. a, The diagram of using the MT to track the unfolding and refolding conformational switch of the N-SH2 C-SH2 region in SHP2 under 8 pN, 8.5 pN, or 9 pN constant forces. **b**, The dynamics of the unfolding and refolding conformational switch of the N-SH2 and C-SH2 domains in SHP2. Switch rates and paths between different conformational states were labelled. Although the experiments were conducted continuously before and after each group, the time axis for each graph was reset to zero, and a 100-second segment was selected for display. SHP2 shown here is core SHP2 (residues: 1–525).

Extended Data Figure 6

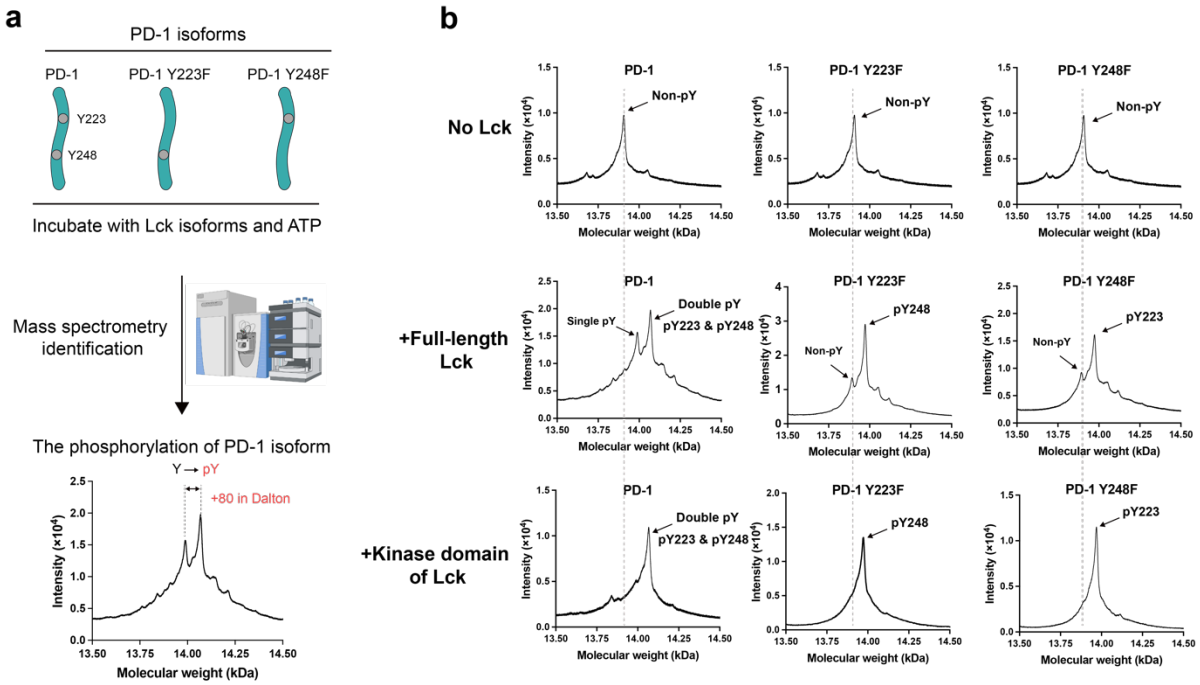

Extended Data Fig. 6 | PD-1 is fully phosphorylated by the kinase domain of Lck. a, The diagram of full-length Lck or the kinase domain of Lck to phosphorylate PD-1, and the subsequent phosphorylation identification by mass spectrometry. **b**, Validation of the phosphorylation of PD-1. PD-1 shown here is the PD-1 intracellular region (residues: 192–288).

Extended Data Figure 7

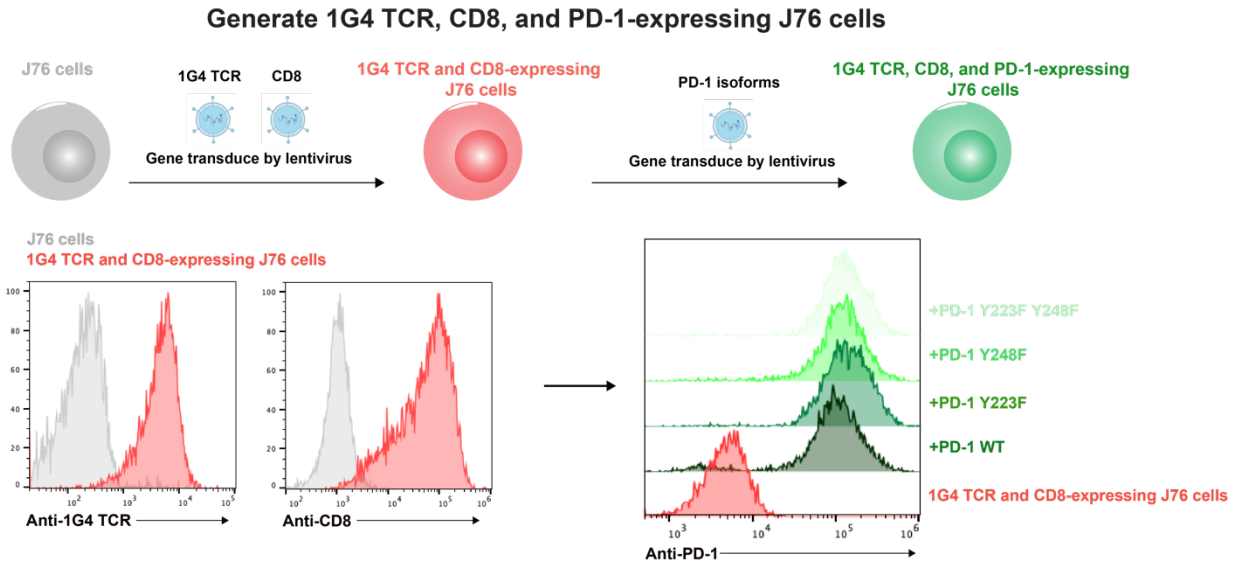

Extended Data Fig. 7 | Generation of 1G4 TCR, CD8, and PD-1-expressing J76 cells.

Extended Data Figure 8

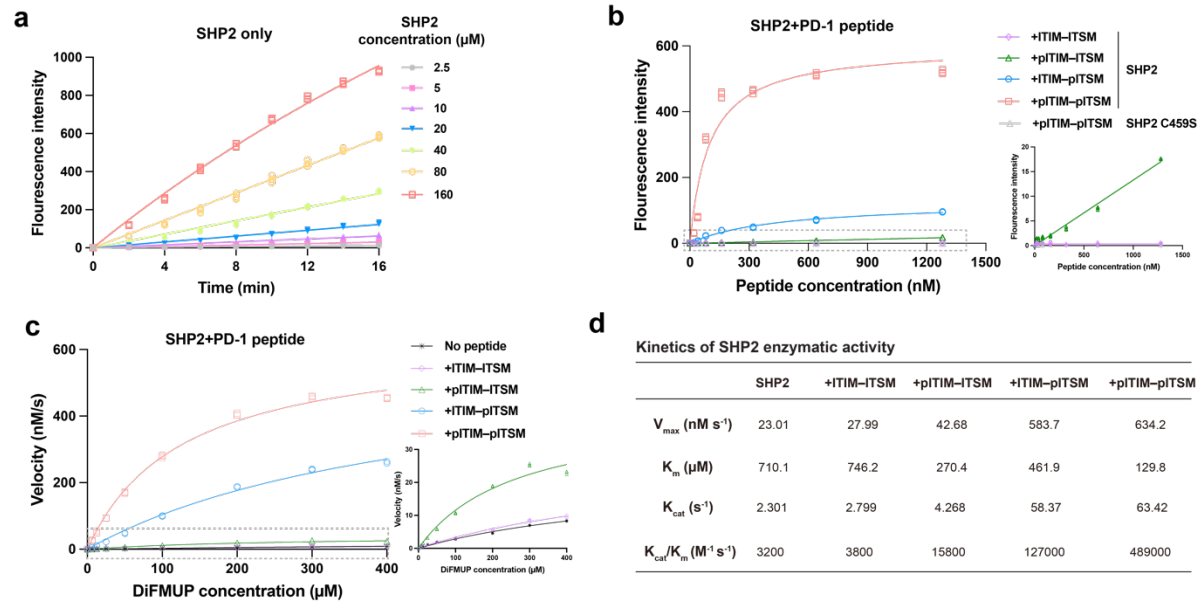

	SHP2	+ITIM–ITSM	+pITIM–ITSM	+ITIM–pITSM	+pITIM–pITSM
V_{max} (nM s^{-1})	23.01	27.99	42.68	583.7	634.2
K_m (μM)	710.1	746.2	270.4	461.9	129.8
K_{cat} (s^{-1})	2.301	2.799	4.268	58.37	63.42
K_{cat}/K_m (M^{-1} s^{-1})	3200	3800	15800	127000	489000

Extended Data Fig. 8 | The phosphorylation of PD-1 regulates SHP2 enzymatic activity. a, The time- and concentration-dependent enzymatic activity of SHP2. 20 μM DiFMUP was shown (*N* = 3, *n* = 3). **b**, The enzymatic activity of SHP2 in the presence of increasing amounts of phosphorylated PD-1 was measured at the 5-minute time point. 10 nM SHP2 and 20 μM DiFMUP were shown (*N* = 3, *n* = 3). **c**, The PD-1 phosphorylation-mediated enzymatic velocity of SHP2 was measured at the 5-minute time point. 10 nM SHP2 and 1 μM PD-1 motif were shown (*N* = 3, *n* = 3). **d**, The measured kinetics of SHP2 enzymatic activity. SHP2 shown here is core SHP2 (residues: 1–525). (p)ITIM–(p)ITSM motif (residues: 218–256, sequence: FSVD(p)YGELDFQWREKTPEPPVPCVPEQTE(p)YATIVFPS). pITSM motif (residues: 242–256, sequence: VPEQTEpYATIVFPSG). pITIM motif (residues: 218–234, sequence: VFSVDpYGELDFQWREKT).

Extended Data Figure 9

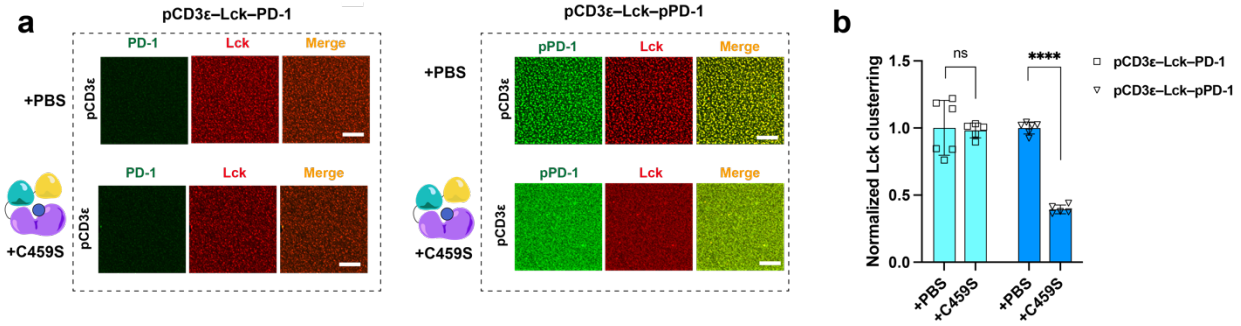

Extended Data Fig. 9 | Non-catalytic SHP2 disrupts the LLPS formed by Lck–pCD3ε–pPD-1. a, Representative confocal images of LLPS formed by Lck–pCDε–pPD-1 with the addition of SHP2 C459S or PBS. The more phosphorylation of PD-1, the more integration of PD-1 into LLPS. **b**, The quantified Lck clustering in LLPS with C459S or PBS. C459S significantly disrupts the LLPS depending on the phosphorylation of PD-1 (N = 3, n = 5 or 6). pCD3ε shown here is the intracellular region (residues: 153–207). PD-1 shown here is the intracellular region (residues: 192–288). pPD-1 was generated through the phosphorylation of PD-1 by the kinase domain of Lck. Lck shown here is the region that contains the Unique, SH3, and SH2 domains. SHP2 shown here is core SHP2 (residues: 1–525). Data in (**b**) were presented as mean ± SD. The significance of the difference was determined by an unpaired two-tailed Student's *t*-test: ****P<0.0001, ns represents no significance. Scale bar size: 10 μm.

Extended Data Figure 10

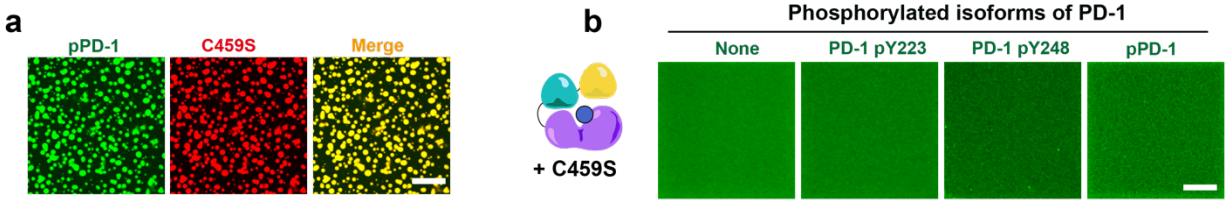

Extended Data Fig. 10 | C459S binds to phosphorylated PD-1 but not to form LLPS on the SLBs. a, High concentration of phosphorylated PD-1 with C459S with PEG in solution. **b**, Low concentration of PD-1 in different phosphorylated states with C459S on SLBs. The C459S shown here is core SHP2 (residues: 1–525) with the C459S mutation. PD-1 shown here is the PD-1 intracellular region (residues: 192–288). Scale bar size: 10 μm.

Extended Data Figure 11

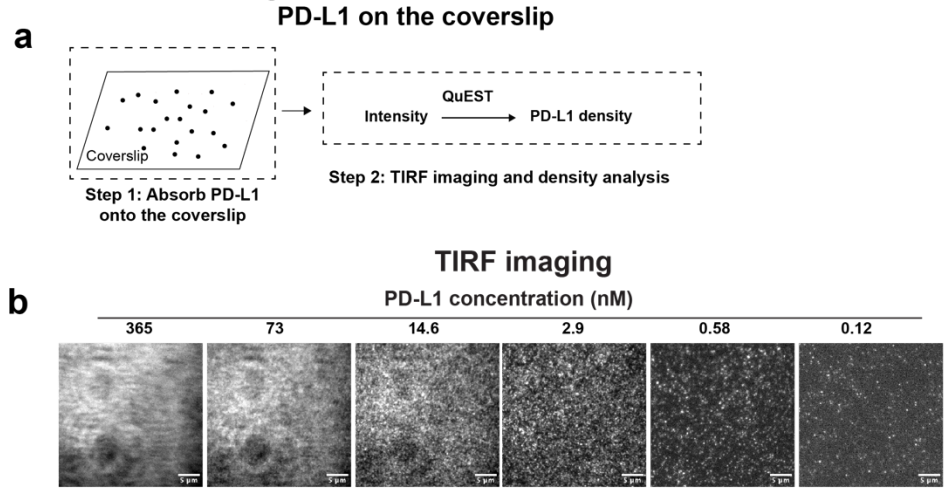

Extended Data Fig. 11 | Quantification of the density of PD-L1 on the coverslip. a, The processes of experiment and quantification. **b**, The representative TIRF images of PD-L1 AF405 on the coverslip.

Extended Data Figure 12

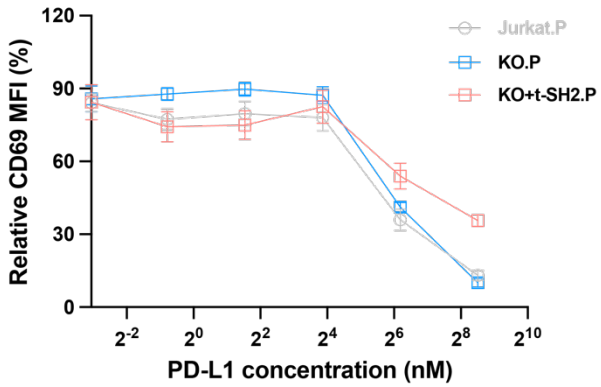

Extended Data Fig. 12 | The PD-1–PD-L1 signaling-regulated activation of Jurkat, SHP2 KO, and KO+t-SH2 cells (*N* = 3, *n* = 6–8).

Extended Data Figure 13

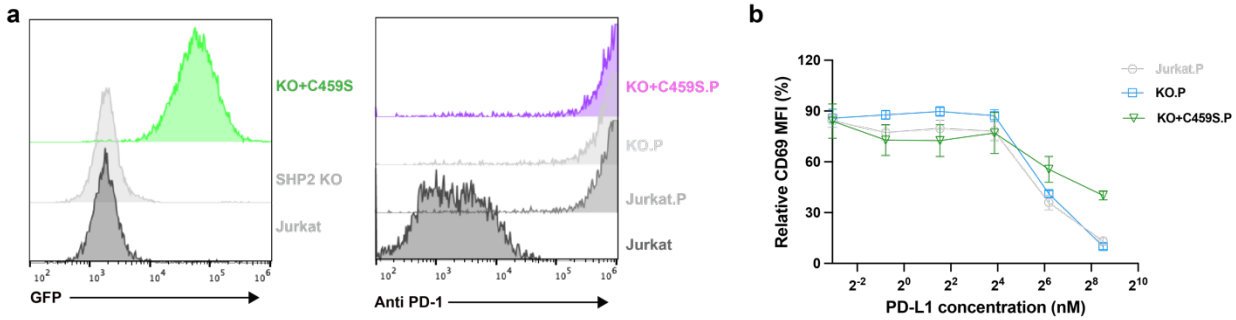

Extended Data Fig. 13 | Generation of KO+C459S.P Jurkat T cells and the PD-1–PD-L1 signaling-regulated cell activation. **a**, Generation of KO+C459S.P Jurkat cells. **b**, The relative CD69 MFI of engineered Jurkat T cells with different PD-L1 concentrations on the surface (N = 3, n = 8).